Latin American Journal of Solids and Structures
www.lajss.org

Optimal Placement of Piezoelectric Macro Fiber Composite Patches on Composite Plates for Vibration Suppression

Abstract

This work presents a new methodology for the parametric optimization of piezoelectric actuators installed in laminated composite structures, with the objective of controlling structural vibrations. Problem formulation is the optimum location of a Macro Fiber Composite (MFC) actuator patch by means the maximization of the controllability index. The control strategy is based on a Linear Quadratic Regulator (LQR) approach. For the structural analysis, the modeling of the interaction between the MFC and the structure is made taking into account the active material as one of the orthotropic laminate shell layers. The actuation itself is modeled as an initial strain arising from the application of an electric potential which deforms the rest of the structure. Thereby, modeling the electric field and the electromechanical coupling within the actuator is avoided because these effects are considered analytically. Numerical simulations show that the structural model presents good agreement with numerical and experimental results. Furthermore, the results show that optimizing the location of the actuator in the structure helps the control algorithm to reduce induced structural vibration.

Keywords

Parametric optimization, macro fiber composite, LQR optimal control, laminated composite material.

Eduardo Padoin [a]
Jun Sergio Ono Fonseca [b]
Eduardo André Perondi [c]
Odair Menuzzi [d]

[a] GMAp – Applied Mechanics Group, R. Sarmento Leite, 425, 90050-170 Porto Alegre, RS, Brazil
email: eduardopadoin@bol.com.br
[b] email: jun@ufrgs.br
[c] email: eduardo.perondi@ufrgs.br
[d] email: odair.menuzzi@ibest.com.br

http://dx.doi.org/10.1590/1679-78251320

Received 29.04.2014
In revised form 13.11.2014
Accepted 15.12.2014
Available online 03.02.2015

1 INTRODUCTION

The increasing demand for light structures in important applications highlights the necessity for using advanced methods in their design, as the structural optimization and optimal control. With sensors and actuators integrated through control systems, these structures have the capacity of sensing environment changes, diagnose localized problems, store and process measured data. They are, then, able to take appropriate action to improve the efficiency of the system or to preserve their structural integrity and safety [Cheng et al. (2008)]. Important applications, according to

Crawley (1994), are systems that can sense induced vibration and, thus, applying forces to control the amplitudes. Smart structures are applied mainly in the aerospace industry, where they can be found, for instance, in flexible robot manipulators [Zimcik and Yousefi (2003)].

The development of methods to design smart structures is a promising research field, fueled by the existing demand for these structures and the great range of possible applications. In the research area of structural design, the topologic and parametric optimization methods contribute efficiently in the design of lighter structures, decreasing costs and the material utilized, evidencing the sustainability aspects of these approaches [Haftka and Gürdal (1991), Bendsøe and Sigmund (2003)].

Optimized structures usually present reduced mass and low internal damping. These features induce the occurrence of structural vibrations, which may cause undesirable operational effects, for instance in positioning accuracy. According to Preumont (2002), the use of an active control system integrated by sensors and actuators is crucial in smart structures. This article presents the application of a specific type of actuator, the MFC (Macro Fiber Composite) piezoelectric transducer [Smart Material (2013)].

The use of piezoelectric ceramics (as the PZT) to generate mechanical force, or, as a sensor in control systems, is relatively well known. When deformed, piezoelectric materials generate an electric charge; conversely they undergo mechanical deformation when subjected to an electric field. As an alternative to monolithic homogeneous ceramic inserts, some composite piezoelectric devices such as the MFC were developed in the last decade. The MFC is a piezoelectric composite actuator and consists in a plane array of PZT rods with wired comb shaped electrodes embedded within polymeric layers. Considering that PZT is a brittle ceramic material, distributing it in thin rods creates a flexible structure, allowing be bonded to curved structures.

This work uses a simplified model to represent the interaction between the MFC and the structure. Most works models the electromechanical effect, where it is necessary to consider the electric field generated between the electrodes, the piezoelectric constitutive model coupling mechanical and electrical systems, resulting thus, in a complex multi-physics model [Latalski (2011), Collet et al. (2010)]. Kapuria et al, 2010, present a review about the development of efficient models and their numerical implementation for piezoelectric laminated plate, especially to dynamics and control, free-edge stresses and micromechanical behavior. Besides, the future challenges in smart composite structure technology are identified.

Differently from others works, we propose here the use of a simpler model to represent the electromechanical interaction, being the structure modeled as a laminate shell and the MFC as orthotropic material layers that present an initial strain. This strain is computed analytically as resulting of the application of an instantaneous electric potential to the electrodes, and it is converted into nodal forces during the finite element discretization. The numerical simulations performed using the proposed approach show that the structural model presents good agreement with numerical and experimental results.

A Linear Quadratic Regulator (LQR) controller is used to the structural vibration control. The dynamic system is represented in state space using modal coordinates [Meirovitch (1990), Preumont (2002) and Gawronski (2004)]. In the active control of structural vibrations using piezoelectric material, the localization of sensors and actuators has significant influence in the

performance of the control system [Kumar e Narayanan, 2008]. Therefore, the present work presents a new parametric optimization methodology that allows the optimal MFC placement by means of the maximization of a controllability index. Sohn et al., 2011, present an optimization technique for shells also using the MFC and a controllability index different from that used in the present work, in which it was used the one proposed by Hac and Liu (1993). [Kang et al. (1996), Quek et al. (2003)], present an optimal placement strategy of piezoelectric sensor/actuator pairs using the maximum damping effect. The optimum location of the sensor/actuator is determined as the point where the structural damping index is maximum.

Based on the aforementioned ideas, this work presents a parametric optimization of piezoelectric actuators on laminated composite structures applied to reduce the structural vibration induced by external forces. In comparison with other optimization forms, the proposed parametric optimization helps to determine the optimal region to bond a commercially available fixed dimension MFC patch in the structure.

2 MACRO FIBER COMPOSITE

The studies about piezoelectric ceramics for actuation and sensing are relatively advanced. However, PZT presents significant restrictions that appear in some actual applications. The PZT is a brittle material, requiring additional attention during the handling and assembly or bonding procedures. Besides, its use in curved surfaces is difficult and may require additional treatment [Kolovos et al. (2007)].

Composite piezoceramic actuators, which have been extensively studied in the last years, can overcome these limitations. The MFC is one these solutions [Smart Material (2013)]. It was developed by NASA for applications in which the structure flexibility prevails at expense of the force capacity. It was developed to be used as sensor and actuator in vibration control and for energy harvesting applications.

The MFC is constituted of rectangular piezoceramic rods sandwiched between layers of adhesive material, electrodes and polyimide film, as shown in Figure 1. The electrodes are attached to the film in an interdigitated pattern which transfers the applied voltage directly to and from the ribbon shaped rods. This assembly enables in-plane poling, actuation and sensing in a sealed and durable, ready to use device. As a thin, surface conformable sheet, it can be applied (normally bonded) to various types of structures or embedded in a composite structure. If voltage is applied, it can be used to bend or distort structures, generate or counteract vibrations. If no voltage is applied, it can work as a strain gauge, sensing deformations, noise and vibrations.

Only one MFC transducer is considered in this work, using the d_{33} effect [Collet et al. (2010), Latalski (2011)] where the strains occur in the same direction of the electrical field. In Fig. 2, it is possible to observe its actuation mode, electrical field direction and polarization.

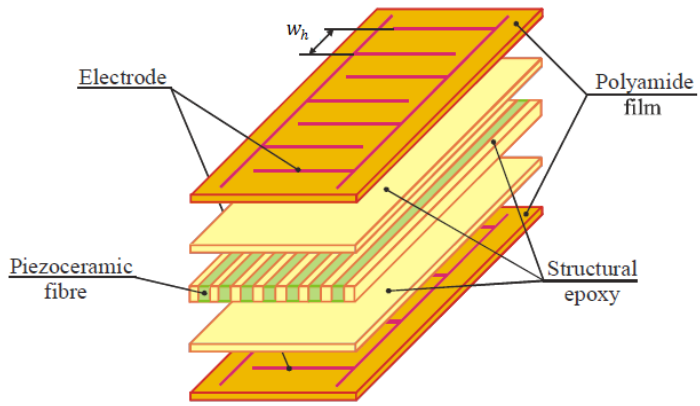


Figure 1: MFC actuator construction, Kovalovs et al.(2007).

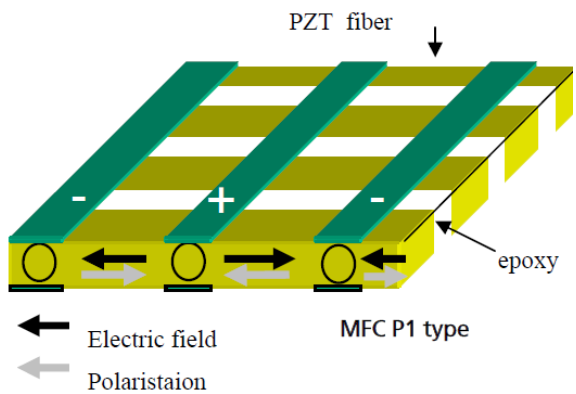


Figure 2: Electrical field and polarization for d_{33} MFC effect, Schönecker et al. (2006).

Figure 3 (right) presents the configuration of the electrodes, which alternates the polarizations in the same surface. Thus, alternating the poles length wise, they are able to produce the electrical field; and, since the polarization is similarly induced, the rods elongate in the 3 orthogonal directions (Figure 3– left).

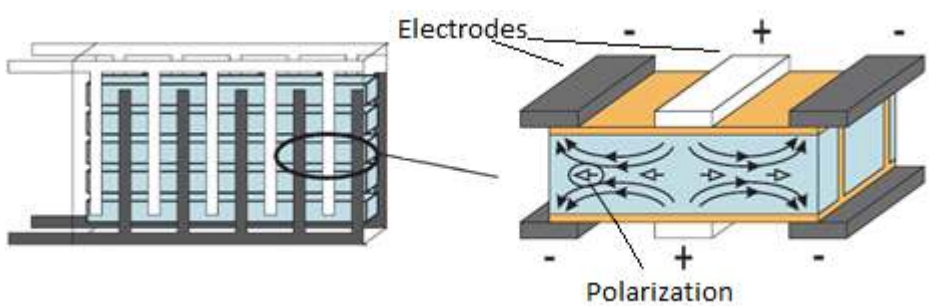


Figure 3: Schema of electrodes and d_{33} MFC effect polarization, Schröck et al.(2011).

3 STRUCTURAL MODELING

The standard approximated solution of the solid mechanics equilibrium equations uses finite element method (FEM) formulation. It uses the assumptions of the infinitesimal linear elasticity and a lamination theory for the composite materials. Mass and stiffness matrices are derived for an eight node serendipity quadrilateral shell element. The element is based on the degenerated solid formulation by Ahmad et al. (1970), and it has five degrees-of-freedom (three displacements and two slopes) per node. A good review of this element can be found in Zienkiewicz and Taylor (2000). The laminated composite part is accounted using an explicit integration through the thickness.

3.1 First-order Shear Deformation Laminated Theory

The First Order Deformation Laminated Theory (FSDT) is based on the Mindlin-Reissner plate theory. It is assumed that a transverse normal segment does not necessarily remain perpendicular to the midsurface after the deformation. The model allows transverse shear strains with linear variation through the thickness [Reddy (2004)]. According Zhang and Yang (2009), the FSDT offers a good compromise between computation efficient and accuracy of the global structural behavior in comparison with the Classical Lamination Theory (CLT). In this theory, the constitutive equation of laminated plate is described as:

$$\begin{Bmatrix} \boldsymbol{N} \\ \boldsymbol{M} \end{Bmatrix} = \begin{bmatrix} \boldsymbol{A} & \boldsymbol{B} \\ \boldsymbol{B} & \boldsymbol{D} \end{bmatrix} \begin{Bmatrix} \varepsilon \\ \kappa \end{Bmatrix}, \tag{1}$$

where N and M are the distributed normal tractions and moments applied to the plate, respectively. The terms ε are referred to the midplane (membrane) strains, while κ corresponds to the curvatures terms.

The matrix $\boldsymbol{A}$ is the extensional stiffness matrix that relates the extensional midplane strain ε with the plate traction $\boldsymbol{N}$. It is written as:

$$\boldsymbol{A} = \sum_{k=1}^{n} \bar{\boldsymbol{Q}}_k (z_{k+1} - z_k), \tag{2}$$

where z_k is the distance from laminate midplane to the bottom of the each k-th layer, $\bar{\boldsymbol{Q}}_k$ is the transformed stiffness matrix and n is the number of layers.

The stiffness matrix $\boldsymbol{B}$ represents the coupling between bending and membrane tension forces, which contains the contribution of the curvature κ in the traction. When the plate is symmetric, $\boldsymbol{B} = \boldsymbol{0}$. This matrix is given by:

$$\boldsymbol{B} = \frac{1}{2} \sum_{k=1}^{N} \bar{\boldsymbol{Q}}_k (z_{k+1}^2 - z_k^2)\,. \tag{3}$$

The matrix $\boldsymbol{D}$ is the bending stiffness matrix and it can be expressed as:

$$\boldsymbol{D} = \frac{1}{3}\sum_{k=1}^{N} \overline{\boldsymbol{Q}}_k (z_{k+1}^3 - z_k^3)\,. \tag{4}$$

More information about FSDT and CLT can be found in composite material textbooks, as Jones (1999) and Reddy (2004).

3.2 Stiffness and Mass Matrices

The stiffness matrix utilized in this work follows a formulation proposed by Kumar and Palaninathan (1997), using an explicit integration on the thickness direction. The elemental transverse integration is accomplished using the third model presented in that paper, in which the inverse isoparametric mapping Jacobian matrix is assumed as being constant, and its computations is executed only on the reference surface.

Therefore, considering that the stiffness matrix can be described by

$$\boldsymbol{K}_e = \int_{\Omega_e} \boldsymbol{F}^T \boldsymbol{C} \boldsymbol{F}\, d\Omega_e\,, \tag{5}$$

where $\boldsymbol{C}$ is the laminated stiffness matrix, and e is the element index. The strain matrix $\boldsymbol{F}$ is divided in two parts that are not dependent on the thickness, and can be rewritten as

$$\boldsymbol{F} = \boldsymbol{F}_1 + z\boldsymbol{F}_2. \tag{6}$$

Using Equation 6, the elementary stiffness matrix can be rewritten as

$$\boldsymbol{K}_e = \int_{-1}^{+1}\int_{-1}^{+1} [\boldsymbol{F}_1^T \boldsymbol{A} \boldsymbol{F}_1 + \boldsymbol{F}_1^T \boldsymbol{B} \boldsymbol{F}_2 + \boldsymbol{F}_2^T \boldsymbol{B} \boldsymbol{F}_1 + \boldsymbol{F}_2^T \boldsymbol{D} \boldsymbol{F}_2]\, |J| d\eta d\xi\,, \tag{7}$$

where the matrices $\boldsymbol{A}$, $\boldsymbol{B}$ and $\boldsymbol{D}$ were already defined in the section 3.1 and $|J|$ is the Jacobian determinant. In this work, we use of a lumped mass matrix, which can be expressed as:

$$\boldsymbol{M}_e = \int_{\Omega_e} \boldsymbol{N}^T \gamma \boldsymbol{N}\, d\Omega_e\,, \tag{8}$$

$$\begin{cases} N_i \gamma N_j\,, & if \quad i = j \\ 0\,, & if \quad i \neq j\,, \end{cases} \tag{9}$$

where γ is the density of the material and $\boldsymbol{N}$ is the interpolation functions matrix for the Ahmad element, being the terms related to the rotational inertia disregarded (Eq. 9). The global stiffness and mass matrices are assembled by a conventional FEM superposition procedure.

3.3 Distributed Force Vector Due to the MFC

As already mentioned, a simplified model is proposed to represent the interaction between the MFC actuator and the structure. This approach presents the advantage of needing less implementation efforts than the alternative based on the modeling of the electric fields and electromechanical effect. Assuming that the MFC is modeled as one of the orthotropic material layers of the laminate shell, it is considered that an additional elemental force vector of distributed loads is obtained from an initial strain existent in the MFC. This strain is proportional to the electrical potential applied in the MFC. Therefore, it is not necessary to model the electric field and the electromechanical coupling, because these effects are considered analytically. Both the stiffness and the mass of the MFC are taken into account in the structural model.

The force vector of the distributed loads on the shell surface can be obtained by means of the following equation

$$\boldsymbol{\varepsilon}^0 = \boldsymbol{\varepsilon}_{MFC}\boldsymbol{\phi} \ , \tag{10}$$

where $\boldsymbol{\varepsilon}_{MFC}$ is the MFC strain vector and $\boldsymbol{\phi}$ is the electric potential.

The strain vector is represented by $\boldsymbol{\varepsilon}_{MFC} = (\varepsilon_{xx}^{MFC}, -v_{12}\varepsilon_{xx}^{MFC}, \varepsilon_{zz}^{MFC}, 0,0,0)$, where ε_{zz}^{MFC} is obtained considering the laminar membrane stress state for orthotropic material. The MFC free strain in direction x is obtained using the following equation

$$\varepsilon_{xx}^{MFC} = d_{33}/w_h \ , \tag{11}$$

where d_{33} is the piezoelectric constant and W_h is the distance between the MFC electrodes.

Multiplying the initial strain $\boldsymbol{\varepsilon}^0$(Eq. (10)) by the laminate stiffness matrix $\boldsymbol{C}$, Eq. (1) yields the mechanical stress associated with this strain. Multiplying the result by the interpolation functions matrix $\boldsymbol{F}$ and integrating on the element reference surface, it is possible to find the nodal forces values for this element,

$$\boldsymbol{f}_d = \int_{\Omega_t} \boldsymbol{\varepsilon}^{0^T} \boldsymbol{C}\, \boldsymbol{F} d\Omega_t \, . \tag{12}$$

Hence, the distributed force vector in the surface of each element can be written as

$$\boldsymbol{f}_d = \int_{-1}^{+1}\int_{-1}^{+1} \left[\boldsymbol{\varepsilon}^{0^T}\boldsymbol{A}\boldsymbol{F}_1 + \boldsymbol{\varepsilon}^{0^T}\boldsymbol{B}\boldsymbol{F}_2\right] |J|\, d\xi\, d\eta \ . \tag{13}$$

Depending on the curvature and on the position of the MFC layer in the stack, the elemental force vector can contain only membrane contributions, or, more likely, also bending moments and shear forces.

4 STRUCTURAL CONTROL

A strategy based on the LQR control technique is used to reduce the structural vibrations. The nodal model obtained from FEM is transformed into a modal model through a solution of an

eigenproblem. Accordingly, it is possible to truncate the system for the most relevant vibration modes, allowing that a real time controller could be implemented. Detailed reviews about LQR control and modal model can be found in Preumont (2002) and Gawronski (2004).

4.1 Modal Model

Modal models of structures are represented in modal coordinates [Gawronski, (2004), Meirovitch(1990)]. For simplification purposes, the full modal model can be truncated, assuming that the lower frequency modes are the most important in its time response. Introducing a modal displacement variable $\boldsymbol{\eta}$, the approximate displacement vector can be represented by a modal superposition of the first n modes [Zoric et al. (2012), Becker et al. (2006)], where the value of n is stablished taking into account a compromise between the computational effort *versus* the required model precision. The modal displacement $\boldsymbol{u}$ can, therefore, be represented as:

$$\boldsymbol{u} = \boldsymbol{\Psi\eta} \ , \tag{14}$$

where $\boldsymbol{\Psi}$ is a vibration modes matrix truncated to n modes. To obtain the modal coordinates equations, it is necessary to substitute the Eq. (14) in the motion equation of the controlled structure in nodal coordinates, represented by:

$$\boldsymbol{M}\ddot{u} + \boldsymbol{D}\dot{u} + \boldsymbol{K}u = B_0 u_c + f \ , \tag{15}$$

where B_0 is the input matrix, u_c is the control input vector, $\boldsymbol{M}$ is the mass matrix, $\boldsymbol{D}$ is the damping matrix, $\boldsymbol{K}$ is the stiffness matrix and f is the force vector. Multiplying Eq. (15) by Ψ^Tresults in terms expressed in modal matrices, as the mass $M_m = \Psi^T \boldsymbol{M} \Psi$, the damping $D_m = \Psi^T \boldsymbol{D} \Psi$, and the stiffness $K_m = \Psi^T \boldsymbol{K} \Psi$. Besides, normalizing the resulting equation set in relation to the mass matrix, it is possible to obtain the modal equation as:

$$\ddot{\eta} + 2Z\Omega\dot{\eta} + \Omega^2\eta = B_m u_c + f_m \ , \tag{16}$$

with

$$B_m = M_m^{-1}\Psi^T B_0 f_m = M_m^{-1}\Psi^T f \ ,$$

and

$$\Omega = \begin{bmatrix} \omega_1 & 0 & \cdots & 0 \\ 0 & \omega_2 & \cdots & 0 \\ \vdots & \vdots & \ddots & \vdots \\ 0 & 0 & ... & \omega_{n_m} \end{bmatrix} \quad Z = \begin{bmatrix} \zeta_1 & 0 & \cdots & 0 \\ 0 & \zeta_2 & \cdots & 0 \\ \vdots & \vdots & \ddots & \vdots \\ 0 & 0 & ... & \zeta_{n_m} \end{bmatrix}, \tag{17}$$

where Ω is a diagonal matrix of natural frequencies which can be obtained from the modal problem solution. The term ω_i is the natural frequency relative to the i-th vibration mode, Z is a diagonal matrix of the modal damping, and each ζ_i term is the modal damping related to the i-th vibration mode which can be obtained experimentally by means of applying the logarithmic decrement concept [Rao S. S. (2010)].

After the transformation to the modal basis, it is possible to obtain a state space representation by rewriting the state vector as a function of the modal displacements and velocities:

$$x = \begin{Bmatrix} x_1 \\ x_2 \end{Bmatrix} = \begin{Bmatrix} \eta \\ \dot{\eta} \end{Bmatrix}. \tag{18}$$

Accordingly, Eq. (16) can be rewritten as a set of first order equations using the definitions below

$$\begin{aligned} \dot{x}_1 &= x_2 \ , \\ \dot{x}_1 &= -\Omega^2 x_1 - 2\mathrm{Z}\Omega x_2 + B_m u_c + f_m, \end{aligned} \tag{19}$$

leading to the following set of equations in state-space form

$$\begin{aligned} \dot{x} &= Ax + B_\phi u_c + f \ , \\ y &= Cx \ , \end{aligned} \tag{20}$$

Introducing the mechanical force vector f_m, the state matrices become:

$$\boldsymbol{A} = \begin{bmatrix} 0 & I \\ -\Omega^2 & -2\mathrm{Z}\Omega \end{bmatrix} \quad \boldsymbol{B_\phi} = \begin{bmatrix} 0 \\ B_m \end{bmatrix} \quad \boldsymbol{f} = \begin{bmatrix} 0 \\ f_m \end{bmatrix} \quad e \quad \boldsymbol{C} = [1 \quad 0] \ ,$$
$$B_m = \Psi^T f_d, \qquad f_m = \Psi^T f \ , \tag{21}$$

where f_d is the mechanical force vector applied to the structure through the MFC actuator.

4.2 LQR Optimal Control

The LQR method is based on the minimization of a quadratic performance index that is associated with the energy of the state variables and control signals [Preumont (2002), Gawronski (2004)]. The goal of LQR controller design is a compromise between the energy state and control by minimizing a cost function defined by

$$J = \int_0^{t_f} (\boldsymbol{x}^T \boldsymbol{Q} \boldsymbol{x} + \boldsymbol{u}^T \boldsymbol{R} \boldsymbol{u}) dt \ , \tag{22}$$

where, $\boldsymbol{x}$ is the state vector, $\boldsymbol{Q}$ is a real symmetric or Hermitian positive definite or positive semidefinite weight matrix for the state variables and $\boldsymbol{R}$ is a Hermitian or real symmetric positive definite matrix which expresses the energy expenditure by the control signal [Preumont (2002)]. It is assumed in this problem that the control vector $\boldsymbol{u}(t)$ is unbounded. A sensible control design must make a consistent choice for these matrices. A widely used choice is the identity matrix or its multiples.

In the LQR approach [Preumont (2002)], an optimal control law can be expressed through Eq. (23):

$$\boldsymbol{u} = -\boldsymbol{G}\boldsymbol{x} \ . \tag{23}$$

If the matrix of elements $\boldsymbol{G}$ is determined to minimize the performance index (Eq. 22), then $\boldsymbol{u}(t)$ is suitable for any initial state $\boldsymbol{x}(\boldsymbol{0})$.

In the standard LQR approach, the optimal gain matrix is expressed by $\boldsymbol{G} = -\boldsymbol{R}^{-1}\boldsymbol{B}^T\boldsymbol{P}$, where $\boldsymbol{P}$ is the solution of the Riccati equation:

$$\boldsymbol{A}^T\boldsymbol{P} + \boldsymbol{P}\boldsymbol{A} - \boldsymbol{P}\boldsymbol{B}\boldsymbol{R}^{-1}\boldsymbol{B}^T\boldsymbol{P} + \boldsymbol{Q} = \boldsymbol{0}. \tag{24}$$

Considering a state feedback control, the closed-loop state equation is, hence, given by:

$$\dot{\boldsymbol{x}} = (\boldsymbol{A} - \boldsymbol{B}\boldsymbol{G})\boldsymbol{x} \ . \tag{25}$$

As a hypothesis, it is assumed that all states are completely measurable or observable and that they are related to the outputs.

For the optimization problem solution, it is necessary to define the system property to be maximized. In the present work, as in Zoric et al. (2012), the optimization task is defined as finding the position for the piezoelectric actuators where the control action spends less energy in the effort dispended to attenuating structural vibrations. Therefore, a performance index associated to the system controllability is adopted. As, for example, in Becker et al. (2006), the measure of the system controllability is performed through the use of the trace of the so-called Gramian controllability matrix W_c, which is defined by the following Lyapunov equation [Preumont (2002)]:

$$\boldsymbol{A}W_c + W_c\boldsymbol{A} + \boldsymbol{B}\boldsymbol{B} = 0 \ , \tag{26}$$

where $\boldsymbol{A}$ and $\boldsymbol{B}$ are the matrices defined in the Eq. (21) and W_c is the Gramian controllability matrix.

5 RESULTS

In order to validate the interaction model between the MFC and the structure presented in the Section 3.3, the static deflection of a fiberglass/epoxy cantilever laminated composite plate resulting from an electrical potential applied to the MFC actuator are compared with the results obtained experimentally by Dano et al. (2007). In this experiment, the actuator (MFC-8523-P1 model) was bonded on a laminated composite plate $[0]_s$, a two-ply unidirectional composite with the ply thickness of 0.165 mm each. The MFC and composite material properties are found in the Apendix I. The plate and MFC dimensions a represented in the Figure 4

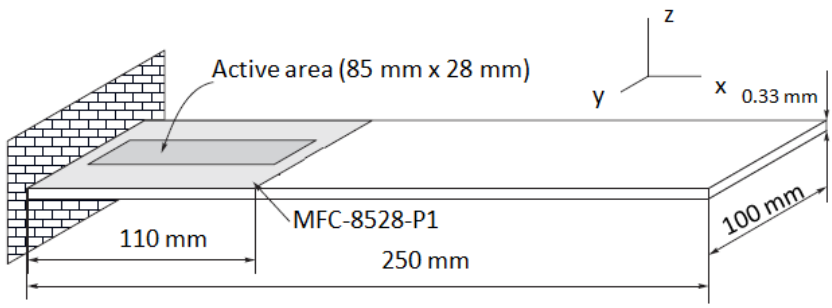


Figure 4: Cantilever laminated composite plate with a MFC actuator bonded to the structure.

The experiment consists in applying an electrical potential of 1000 Volts to the MFC. The structural deflection is measured in some points. Figure 5 presents the values experimentally measured and obtained in this work by simulations using the proposed model.

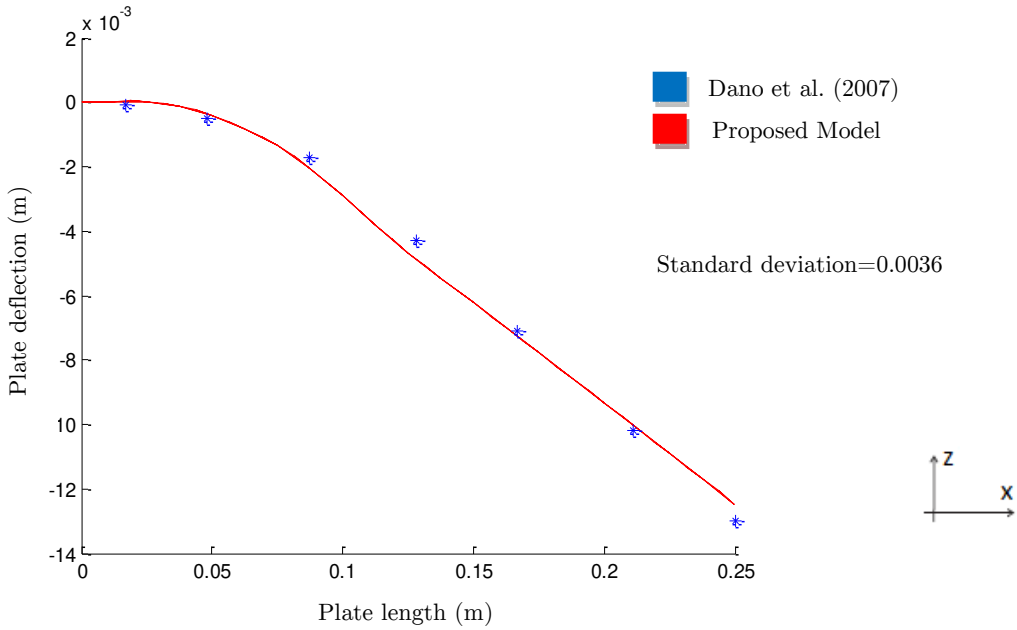


Figure 5: Deflection values obtained through the proposed model and from experiments performed by Dano et al. (2007).

As shown in Figure 5, the results obtained through the proposed model present good agreement with the results obtained in the experimental tests.

Another static displacement analysis using the model of the structure presented in the Figure 6 (Fiberglass/Epoxy) was performed with the application of an electrical potential in the MFC actuator. The actuator (MFC-8523-P1 model) was bonded on a laminated composite plate [0,90], a two-ply composite with the ply thickness of 0.5 mm each. The MFC and composite material properties can be found in the Apendix I.

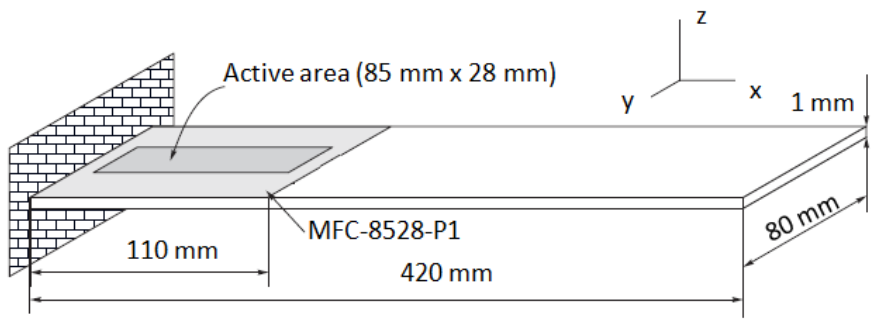


Figure 6: Cantilever laminated composite plate with a MFC actuator bonded to structure (case study).

The structural displacement, correspondent to the application of an electric potential of 1000 volts to the MFC, is shown in the figures 7 and 8.

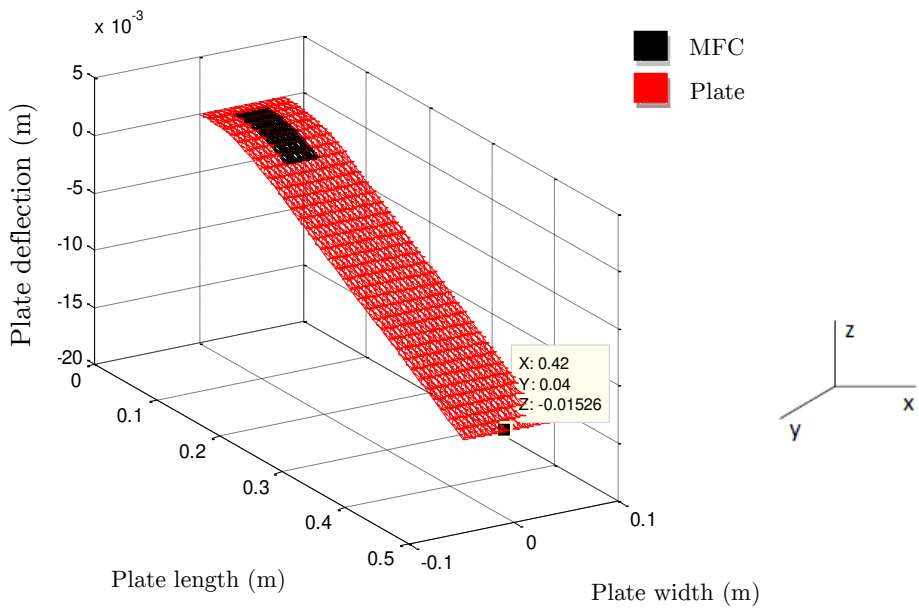


Figure 7: Plate displacement correspondent to an electrical potential of 1000 V.

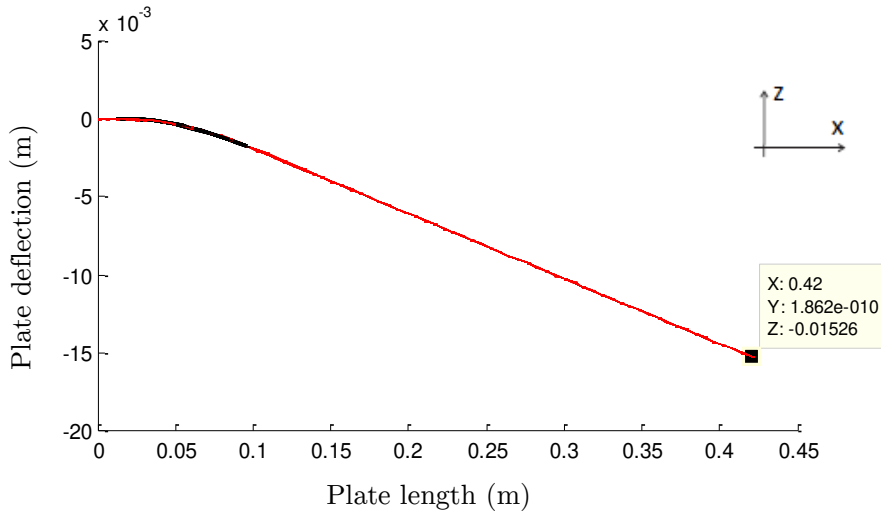


Figure 8: Plate displacement in plane *xz* relative to the application of an electrical potential of 1000 volts.

According to figures 7 and 8, the maximum transverse displacement value is about 15.26mm.

5.1 Optimal Placement

As previously mentioned, in order to find the optimal placement of the MFC actuator to control the structural vibrations, a strategy based on the controllability index (the trace of Gramian controllability matrix) is applied. According to this strategy, the MFC placement is varied along the length of the plate, from the cantilever clamped tip to the free tip, preserving its position centered in the y direction, as presented in Figure 9. In order to simplify the modeling, the gap variation for each new MFC placement is given by the size of each finite element, resulting, in one discrete set of placement candidates.

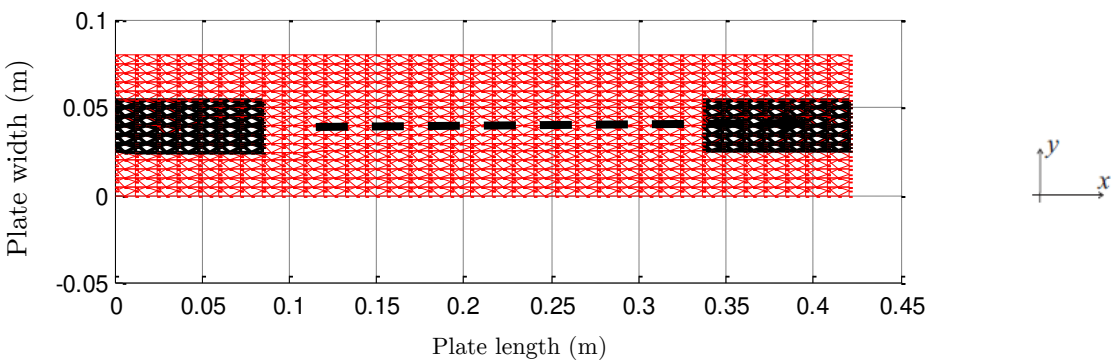


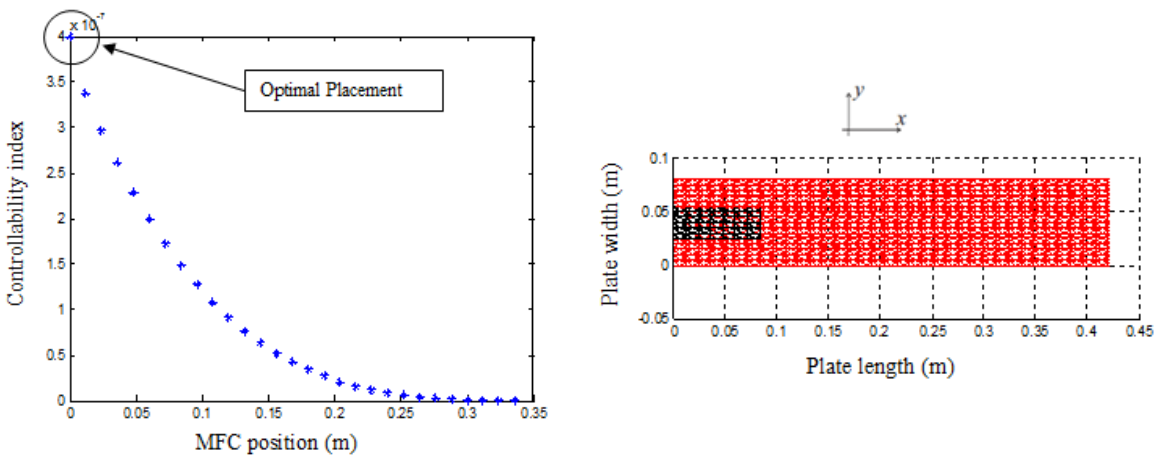
Figure 9: Schema of the MFC placement variation along the length of the plate.

In each new placement, the structural analysis is performed, and, consequently, the controllability index (the trace of the Gramian controllability matrix) is recalculated. It is, therefore, possible to plot the relation between the MFC placement in the structure and the relative controllability index. The objective function is the maximization of the trace of the Gramian controllability matrix and the constraint is the length of the plate

$$\begin{aligned} &max \quad tr(\boldsymbol{W_C}), \\ &subject\ to \left\{ MFCposition + MFC_{length} \leq PLATE_{length}, \right. \end{aligned} \tag{27}$$

where the $\boldsymbol{W_C}$ is the Gramian controllability matrix presented in Section 4.3.

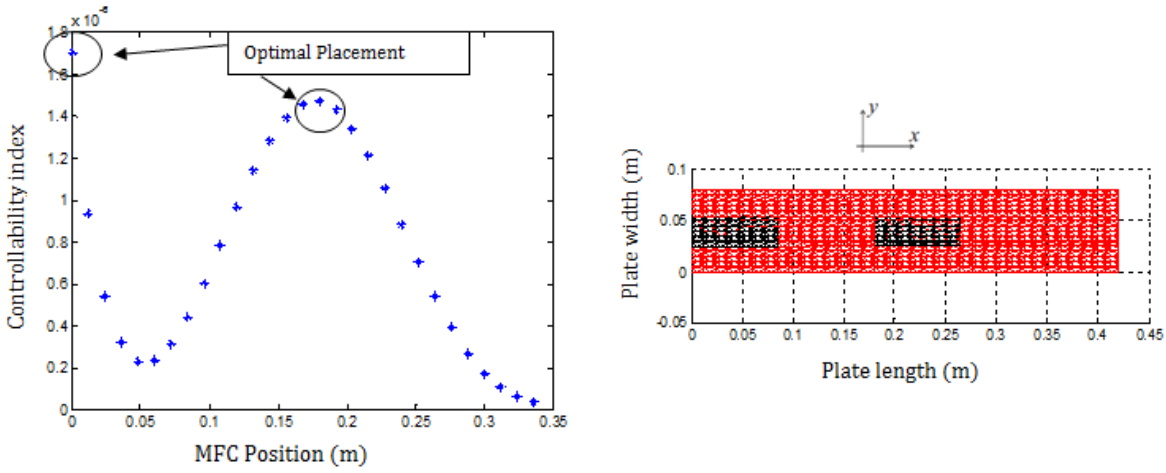
Figure 10 (a) presents the optimal placement index associated to the first bending mode and Figure 10 (b) presents the MFC optimal placement correspondent to the maximized controllability index. Each controllability index from the Figure 10 (a) is related with the left border of the MFC in the plate. The same relation is used for all simulated cases.



(a) (b)

Figure 10: Placement index (a) and optimal placement (b) associated to the first bending mode.

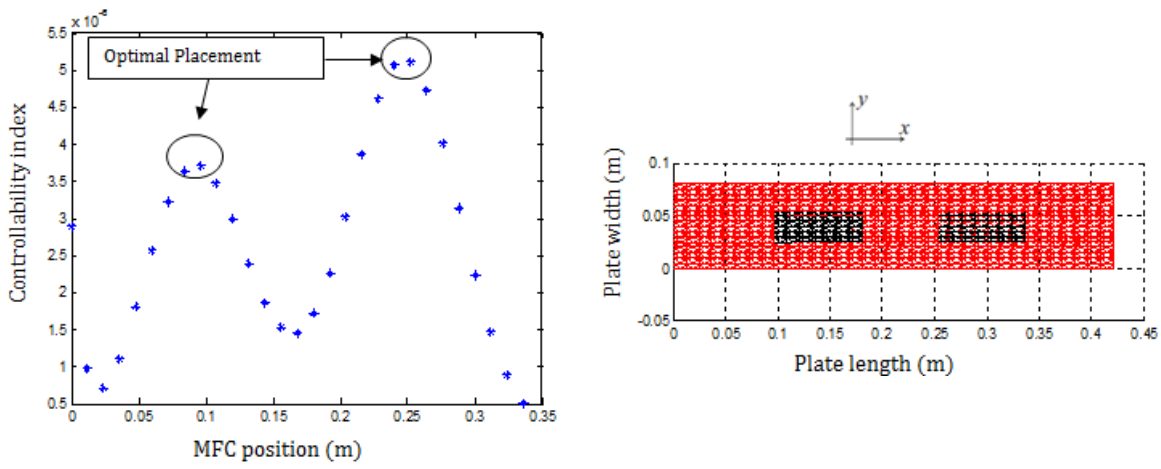
This procedure was repeated for the second and third bending modes of the plate. Figure 11 (a) shows the optimal placement index associated to the first and second bending mode and Figure 11 (b) presents the two regions for optimal MFC placement in the plate. The first optimal place is located in the cantilever tip, and the second position is located between 0.18 m and 0.264 m.



(a) (b)

Figure 11: Placement index (a) and optimal placement (b) to the second bending mode.

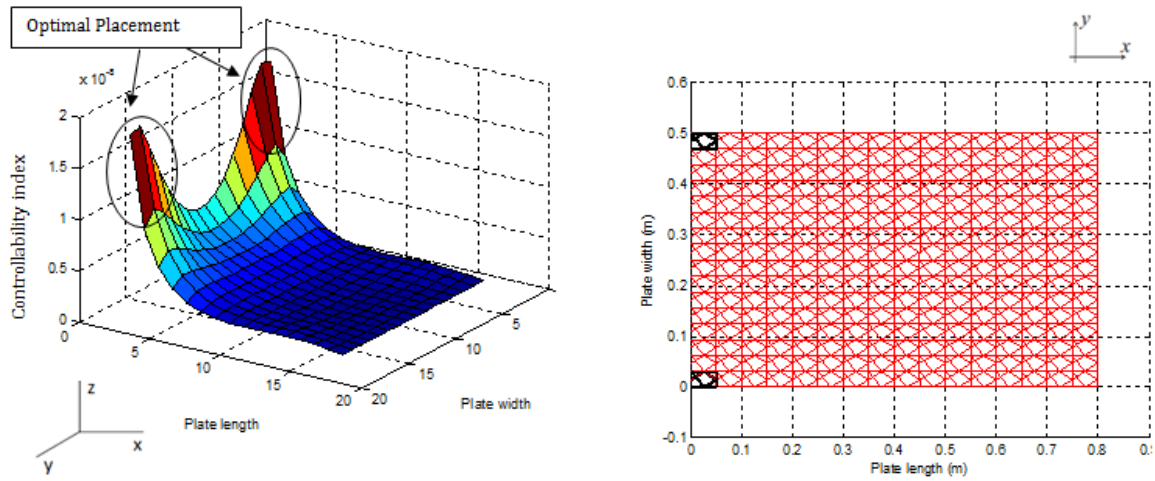
Figure 12 (a) presents the optimal placement index associated to the first three bending modes. It is possible to notice again two places for the optimal MFC placement in the plate. The first place is positioned between 0.096 m and 0.18 m, and the second place is positioned between 0.252 m and 0.336 m. The optimal positions can be visualized in the Figure 12 (b).



(a) (b)

Figure 12: Placement index (a) and optimal placement (b) to the third bending mode.

Another analysis was performed in order to find the optimal placement of the MFC to control the first torsion mode of the plate presented in Figure 6. In this case, the MFC placement is varied in all elements of the plate, from the cantilever tip until the free tip. It is, then, possible to plot the relation between the MFC placement in the structure and the relative controllability index in all the plate. Figure 13 presents the optimal placement index associated to the first torsion mode and the optimal MFC placement associated to the maximization of the controllability index.



(a) (b)

Figure 13: Placement index (a) and optimal placement (b) correspondent to the first torsion mode.

5.2 Behavior of the Controlled Structure

The control algorithm is designed to reduce structural vibrations, decreasing the system overshoot and settling time. The simulations were performed for the case with free tip initial null velocity and a displacement of 0.01 m. The MFC is on the optimal place located closed to the clamped tip. A truncated modal structural model with the five first vibration modes is considered. A structural equivalent damping ratio of 0.018 was obtained experimentally using the logarithm decrement equation [Rao S. S. (2010)].

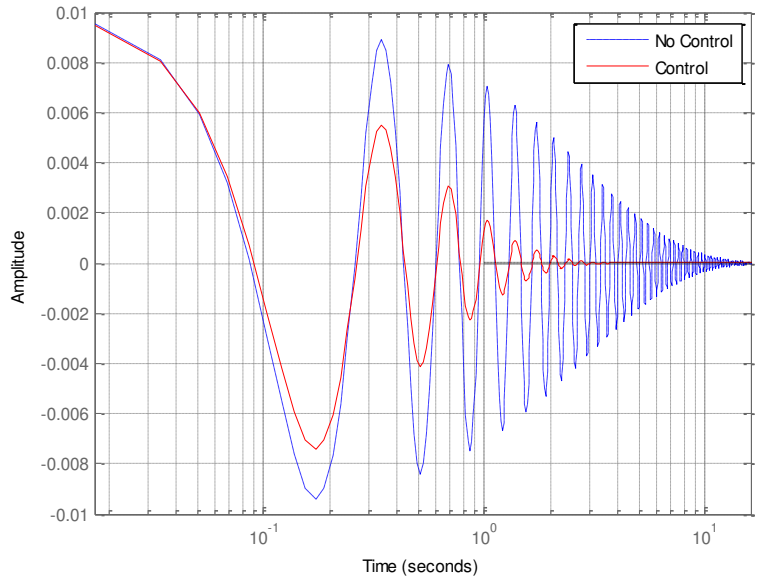
To determine the values of the weighting matrices (Q and R), it was established as choice criterion, the limits of voltage supported by MFC (between -500 and 1500 V), avoiding, thus, the depolarization of the material. However, the criterion does not consider long term effects. Eq. (28) presents the values obtained by this criterion.

$$\mathbf{Q} = 1e8 * [\boldsymbol{I}]_{n\,x\,n}$$
$$\boldsymbol{R} = [4]\,. \tag{28}$$

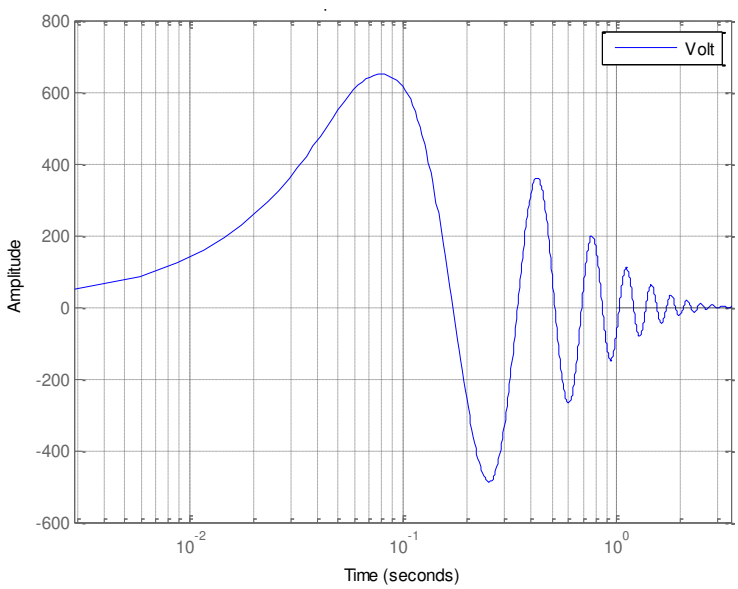
The transverse displacement in free tip was evaluated considering the system in open and closed-loop. Fig. (14) presents the results of the transverse displacement (Fig. 14 (a)) and the control signal applied (Figure 14 (b)), using the values given in Eq. (28). The results indicate that the LQR control system in closed-loop contributes to decrease the displacement amplitude in the free tip. The overshoot and the settling time are also significantly reduced. The maximum value of the applied electric tension is 650 V and the minimum value is -487 V (Figure 14 (b)), both within the actuator operational limits.

Figure 15 presents the response representation in the frequency domain of both open and closed-loop systems. It is possible to verify the decreasing of the amplitudes in the resonance

frequencies in the closed-loop due to the controller influence. This effect is more evident in the first and second bending modes because these modes are that with higher amplitude responses to the given excitation and due to the fact that the MFC optimal placement results in a position for the actuator that is more effective in controlling the vibration associated to this two modes. According to Sohn et al., (2011), optimal configurations of MFC actuators improve the control performance of the smart structures in the cases where a limited number of actuators are available.



(a)



(b)

Figure 14: Transverse displacement of the free tip (m) and control signal (V) relative to the model with five vibration modes.

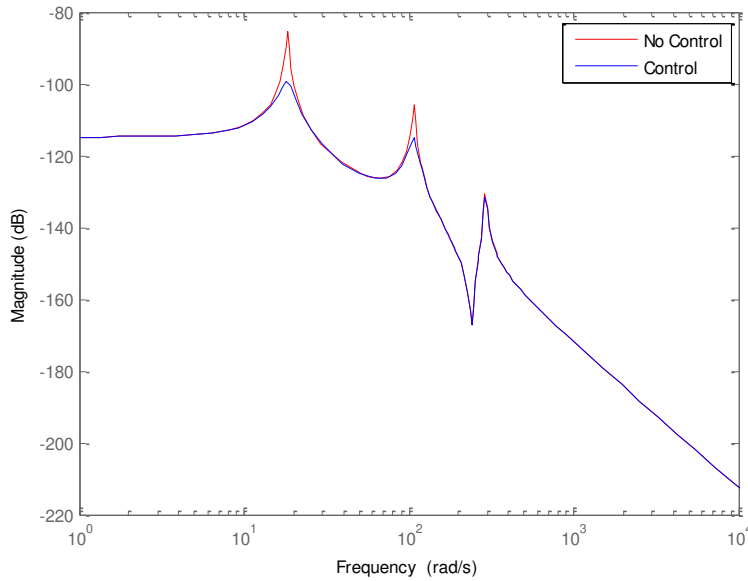
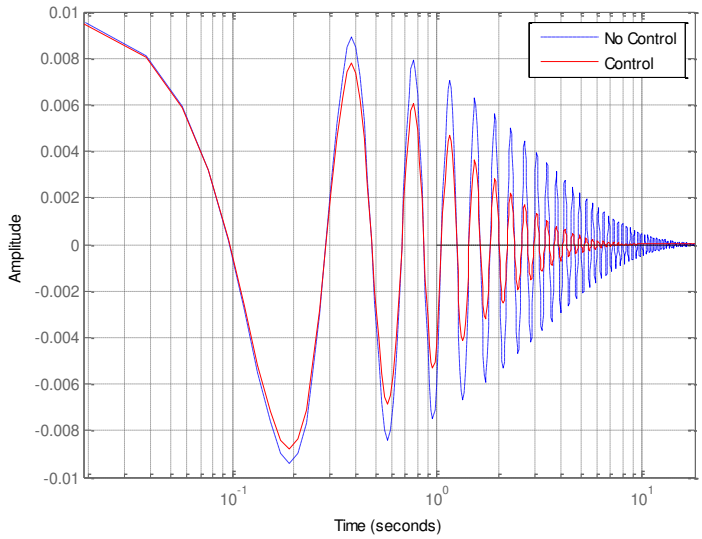


Figure 15: Open and closed-loop frequency responses for the optimal actuator positioning case.

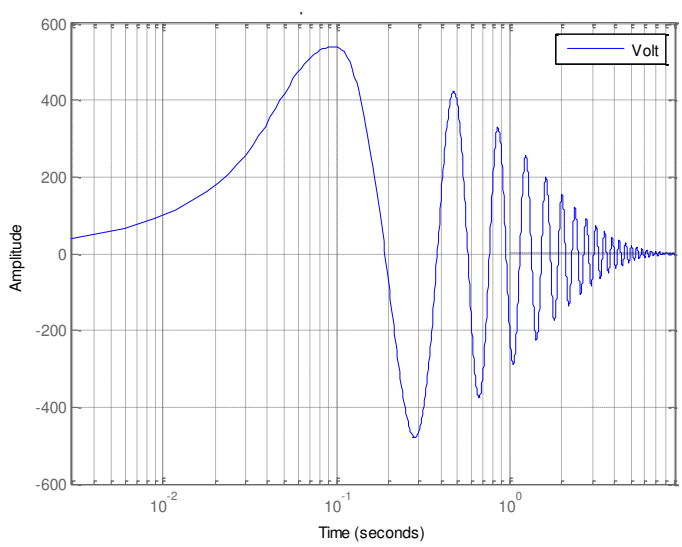
In order to analyze the performance of the system in terms of overshoot and settling time of the controlled plate with the MFC on a non-optimal place, another simulation was performed considering the MFC localized between the positions 0.18 m and 0.264 m. Equation (29) presents the values of the weighting matrices used in this analysis.

$$\mathbf{Q} = 1e8 * [\boldsymbol{I}]_{n\,x\,n}$$
$$\boldsymbol{R} = [3]\,. \tag{29}$$

The transverse displacement in the free tip was evaluated considering the system in open and closed-loop. Figure 16 shows the results of the transverse displacement (Fig. 16 (a)) and the applied control signal (Fig. 16 (b)), utilizing the values given in Eq. (29). The results show that the LQR control system also contributes to decreasing the displacement in the free tip. However, the overshoot and the settling time are bigger than in the previous (optimal) case. Also, the value to electric tension applied to the piezoelectric actuators presents higher amplitudes during the transient displacement (Figure 16 (b)).



(a)



(b)

Figure 16: Transverse displacement of free tip (m) and control signal (V) applied to the model with arbitrary actuators position.

Figure 17 presents the response representation in the frequency domain of both open and closed-loop systems. It is possible to observe that the presence of the controller reduces the amplitude associated to the resonance frequencies in the three first bending modes. However, diversely from the previous (optimal) case, the reduction is more effective in the second bending mode.

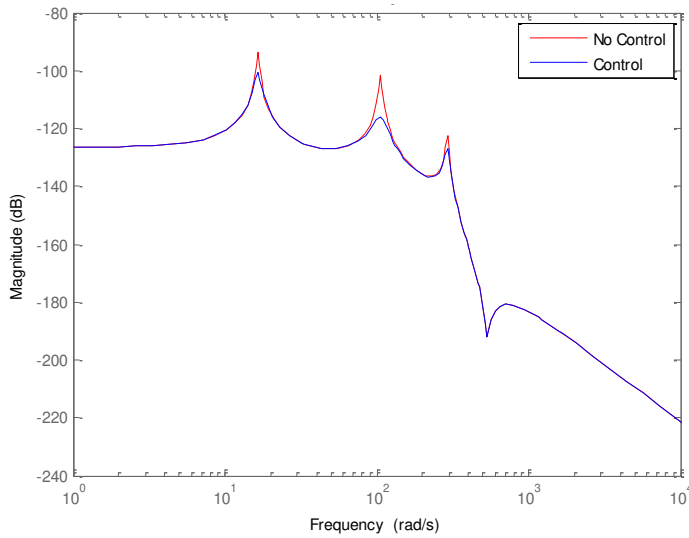


Figure 17: Open and closed-loop frequency responses for a non-optimal actuator positioning case.

6 CONCLUSIONS

The parametric optimization methodology proposed in this article shows by means of simulation and analysis procedures that it is possible to improve the behavior of a controlled structure increasing the MFC capability to control the structural vibrations. The optimization is formulated to determine the optimum localization of the Macro Fiber Composite (MFC) in the active layer through the maximization of a controllability index. Regarding the controlled system behavior, from the simulations responses to an initial position problem, it was possible to design a LQR control that contributes to decrease the structure displacement amplitude along the time. The results showed that the overshoot and the settling time are also significantly reduced with the optimized placement. Furthermore, the maximum and minimum value to electric tension applied was maintained within the MFC operational limits, avoiding the saturation of the control action and the depolarization of the material.

Comparative simulation results showed that the MFC-structure interaction model used presents good agreement with numerical and experimental results from models that take into account the complex electromechanical effect. The results obtained through the use of the proposed model of the MFC-structure interaction are close to that obtained by other researchers, demonstrating that the this strategy can be used in the MFC analysis and optimization.

References

Ahmad, S.; Irons, B. M. and Zienckievicz, O. C. (1970). Analysis of Think and Thin Shell Structure by Curved Finite Elements, International Journal for Numericas Methods in Engineering, vol, 2, p. 419-451.

Becker, J.; Fein, O.; Maess, M. and Gaul, L.(2006). Finite element-based analysis of shunted piezoelectric structures for vibration damping, Computers and Structures, Vol. 84, p. 2340–2350.

Bendsøe, M. e Sigmund, O. (2003). Topology Optimization - Theory, Methods and Applications. Springer, Berlin.

Cheng, Y. F.; Jiang, H. and Lou K. (2008). Smart Structures: Innovative Systems for Seismic Response Control.

Collet, M.;Ruzzene, M.; Cunefare, K. and Xu, B. (2010). Modeling and Characterization of Macro-Fiber Composite Transducers for Lamb Wave Excitation, Health Monitoring of Structural and Biological Systems.

Crawley, E.F. (1994). Intelligent Structures for aerospace: A technology overview and assessment, AIAA Journal, Vol. 32. P. 1689-1699.

Dano, M. L.; Gakwaya, M. and Julliè Re, B. (2007). Compensation of Thermally Induced Distortion in Composite Structures using Macro-fiber Composites, Journal of Intelligent Material Systems and Structures.

Gawronski, W. (2004). Advanced Structural Dynamics and Active Control of Structures. Springer, New York.

Hac A, Lui L. (1993). Sensor and actuator location in motion control of flexible structures. Journal of Sound and Vibration.V. 167(2), pp. 239–261.

Haftka, R. and Gürdal, Z. (1991). Elements of Structural Optimization. Kluver Academic Publishers, 3rd edition.

Jones, R. M. (1999). Mechanics of Composite Materials. Scripta Book Company, Washington, 2nd edtion.

Kang K. Y.; Park H. C.; Hwang W.; Han K. S. (1996). Optimum Placement of Piezoelectric Sensor/Actuator for Vibration Control of Laminated Beams. AIAA Journal, Vol. 34.

Kapuria S.; Kumari P.; Nath J. K. (2010). Efficient modeling of smart piezoelectric composite laminates: a review, Acta Mechanical

,vol. 214, Issue 1-2, pp 31-48.

Kovalovs A.; Barkanov E.; Gluhihs S. (2007). Active control of structures using macro-fiber composite (MFC), Journal of Physics: Conference Series 93.

Kumar, R. and Narayanan, S. (2008). Active vibration control of beams with optimal placement of piezoelectric sensor/actuator pairs, Smart Materials and Structures, vol. 17, pp. 01–15.

Kumar, W. P. P. and Palaninathan, R. (1997). Finite Element Analysis of Laminated Shells with Exact Through-Thickness Integration, Computers and Structures, Vol, 63(1), p.173-184.

Latalski, J. (2011). Modelling of macro fiber composite piezoelectric active elements in ABA QUS system, Maintenance And Reliability NR 4.

Meirovitch, L. (1990). Dynamics and Control of Structures. John Wiley & Sons, New York.

Preumont, A. (2002).Vibration Control of Active Structures, An Introduction. Kluwer.

Quek S. T.; Wang S. Y.; Ang K. K. (2003). Vibration Control of Composite Plates via optimal Placement of Piezoelectric Patches. Journal of Intelligent Material systems and Structures, Vol. 14.

Rao. S. S. (2010).Mechanical Vibrations. Prentice Hall, 3 thedition.

Reddy, J. N. (2004). Mechanics of Composite Plates and Shells – Theory and Analysis. John Willey & Sons, Inc.

Schönecker, A. J.; Daue, T.; Brückner, B.; Freytag, C.; Hähne L and Rödig T. (2006). Overview on Macro Fiber Composite Applications, Smart Structures and Materials: Active Materials: Behavior and Mechanics.

Schröck, J.; Meurer, T. and Kugi, A. (2011).Control of a flexible beam actuated by macro-fiber composite patches: I. Modeling and feedforward trajectory control, Smart Materials And Structures, Vol. 20.

Smart Material. (2013). http://www.smart-material.com/MFC-product-main.html. The research was done on March 11.

Sohn, J. W.; Choi, S. B. and Kim, H. S. (2011). Vibration control of smart hull structure with optimally placed piezoelectric composite actuators, International Journal of Mechanical Sciences, Vol. 53, p. 647–659.

Zhang, Y. X. and Yang, Z. h. (2009). Recent Developments in Finite Element Analysis For Laminated Composite Plates, Composite Structures, Vol. 88, p. 147-157.

Zienkiewicz, O. and Taylor, R. L. (2000). The Finite Element Method – Solid Mechanics. Vol. 2, Elsevier Academic Press, 5th edition.

Zimcik, D. G.; Yousefi-Koma A. (2003). Applications of Smart Structures to Aircraft for Performance Enhancement, Canadian Aeronautics and Space Journal, Vol. 49, p. 163-172.

Zoric N. D.; Simonovic, A. M.; Mitrovic, Z. S. and Stupar, S. N. (2012).Optimal vibration control of smart composite beams with optimal size and location of piezoelectric sensing and actuation, Journal of Intelligent Material Systems and Structures, Vol. 24(4), p. 499–526.

Appendix I

In the table 1 are shows the MFC and composite material properties which are utilized in research of Dano et al. (2007).

COMPOSITE MATERIAL (Fiberglass/Epoxy)	MFC
E_1= 101.6 GPa	E_1= 30.3 GPa
E_2= 7.91 GPa	E_2= 15.9 GPa
E_3= 7.91 GPa	E_3= 11.47 GPa
G_{12}= 3.01 GPa	G_{12}= 5.50 GPa
G_{13} = 3.01 GPa	G_{13} = 2.60 GPa
G_{23}= 2.71 GPa	G_{23}= 2.14 GPa
v_{12}= 0.318	v_{12}= 0.31
v_{13}= 0.318	v_{13}= 0.289
v_{23}= 0.458	v_{23}= 0.327
γ = 1793 kg/m^3	γ = 5440 kg/m^3

Table 1: Properties of the composite material and MFC utilized by Dano et al. (2007).

Where $E_1, E_2 e\, E_3$ are the elastic modulus of material in the directions 1, 2 and 3, respectively, $v_{12}, v_{23} e v_{31}$ are the Poisson coefficients and $G_{12}, G_{23} e\, G_{31}$ are the shear modulus in the planes 1-2, 2-3 and 3-1, respectively.

Table 2 shows the properties of a layer of the plate which was used to validate the numeric model, and the MFC properties, where 1 is the fiber direction;

COMPOSITE MATERIAL (Fiberglass/Epoxy)	MFC
E_1= 29.09GPa	E_1= 30.336 GPa
E_2=E_3 = 8.841 GPa	E_2= E_3= 15.857 GPa
G_{12}=G_{13} = 2.726 GPa	G_{12}= G_{13}= 5.515 GPa
G_{23}= 1.205 GPa	G_{23}= 2.6GPa
v_{12}= v_{13}= 0.1434	v_{12}= v_{13}= 0.31
v_{23}= 0.2933	v_{23}= 0.327
γ = 1793 kg/m^3	γ = 5440 kg/m^3

Table 2: Properties of the composite material and MFC.